Contrasting characteristics of linear-field and cross-field atmospheric plasma jets

J. L. Walsh and M. G. Kong[a)]
Department of Electronic and Electrical Engineering, Loughborough University, Leices LE11 3TU, United Kingdom

(Received 1 August 2008; accepted 26 August 2008; published online 15 September 2008)

This letter reports an experimental study of two types of atmospheric pressure plasma jets in terms of their fundamental properties and their efficiency in etching polymeric materials. The first plasma jet has a cross-field configuration with its electric field perpendicular to its gas flow field, whereas the second is a linear-field device having parallel electric and flow fields. The linear-field jet is shown to drive electron transportation to the downstream application region, thus facilitating more active plasma chemistry there. This is responsible for its etching rate of polyamide films being 13-fold that of its cross-field counterpart. © *2008 American Institute of Physics*.
[DOI: 10.1063/1.2982497]

Atmospheric-pressure glow discharge (APGD) jets are finding increasing success in meeting different requirements of diverse materials processing applications including etching, deposition, nanopatterning, and surface decontamination.[1,2] Typically the feed gas is ionized in an upstream electrode unit, and then the generated plasma is flushed as a plume to a downstream application region where reactive gases are often introduced. APGD jets are easy to construct, and as a result many different jet configurations have been reported. One common type APGD jet employs a coaxial electrode structure with the electric field being largely in the radial direction and the feed gas flowing in the axial direction.[3–5] It is referred here to as the cross-field device as its electric field and its flow field are perpendicular to each other. Very different is another common jet configuration that often employs a powered electrode wrapped around a hollow dielectric tube through which the feed gas flows axially.[6–10] As the flow field and the electric field are parallel, this type of APGD jets is referred to as the linear-field device. Despite of the scale of their applications, there is considerable ambiguity as to their relative merits for materials processing, thus compromising the value of many application-focused studies. The ambiguity also highlights an important knowledge gap in APGD physics and chemistry. In this letter, we report an experimental study on electrical and optical properties of cross-field and linear-field rf APGD jets, as well as their difference in polyamide etching as an example of processing applications.

In our experiments, the cross-field APGD jet had a coaxial configuration with a central powered electrode of 1 mm diameter and a grounded outer electrode wrapped around a 4 mm diameter quartz tube. The linear-field jet consisted of a single powered electrode wrapped around the outside of an identical quartz tube also of 4 mm in diameter. In both cases, helium was flown at a rate of 10 standard l/min and their power electrode was connected to a 4 MHz power supply via a matching network. Electrical measurements were made with a Pearson 2877 current probe and a Tektronix P6015A voltage probe. Optical diagnostics were made using an Andor Shamrock spectrometer with a grating of 2400 grooves/mm.

Figures 1(a) and 1(b) show an image of each plasma jet captured using an Olympus digital camera with 1/30 s exposure combined with an overlaid schematic highlighting their configurations. Both were operated with a fixed input rf power of 15 W and a negligible reflected power. In the case of the cross-field jet, a portion of its outer ground electrode was removed to allow a clear view of the plasma produced between the two concentric electrodes in Fig. 1(a). From the image, it is clear that the discharge appears very intense in the intraelectrode region and much weaker outside the quartz tube. With radiometric calibration using an Ocean Optics LS-1-CAL tungsten halogen light source, Fig. 1(c) suggests that its absolute optical emission intensity, integrated from 250 to 850 nm, reduces monotonically by 5.4-fold from 27.0 mW/cm^2 at $z=0$ mm to 5.0 mW/cm^2 at $z=10$ mm. Its plume is about 7.9 mm outside the quartz tube ending at $z=12.9$ mm. By contrast, the linear-field APGD jet in Fig. 1(b) is less intense inside the quartz tube with a wavelength-integrated optical intensity of 20.1 mW/cm^2 at $z=0$ mm, or 74% of 27.0 mW/cm^2 for the cross-field case. However its intensity remains high over a longer plume length of 12.6 mm outside the quartz tube. Figure 1(c) suggests that its wavelength-integrated emission intensity reaches its maxi-

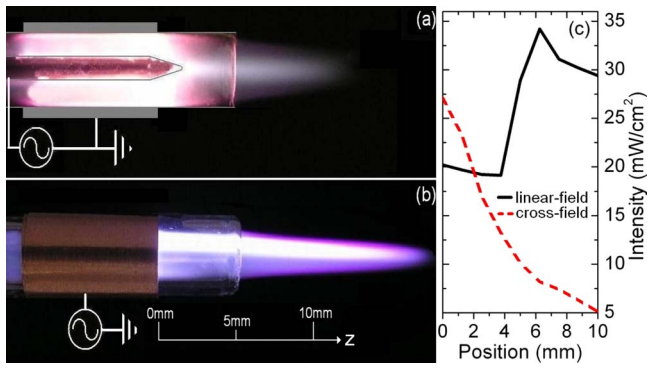

FIG. 1. (Color online) Image showing (a) a cross-field plasma jet and (b) a linear-field jet with (c) the spatial dependence of their wavelength-integrated optical emission on the axial direction. Both jets were sustained at 15 W input rf power.

[a)]Author to whom correspondence should be addressed. Electronic mail: m.g.kong@lboro.ac.uk.

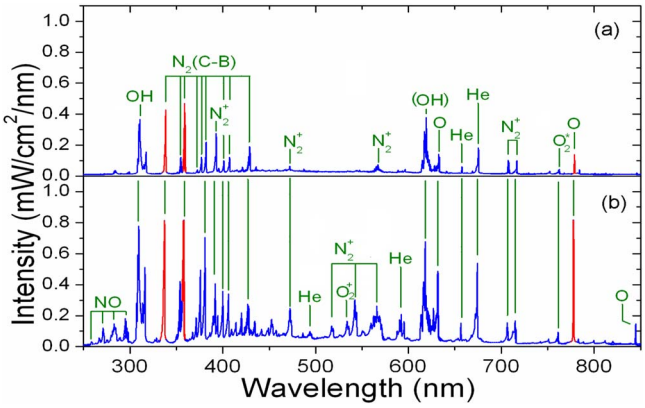

FIG. 2. (Color online) Absolute optical emission of (a) the cross-field jet and (b) the linear-field jet under the same condition as in Fig. 1. Strongest lines are marked in red.

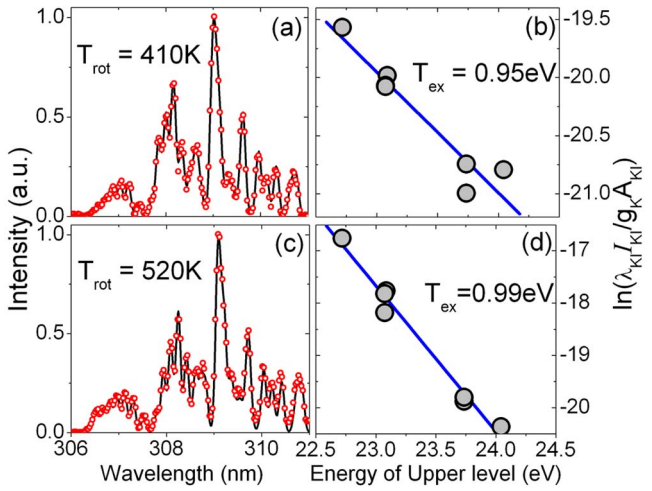

FIG. 3. (Color online) Measured and simulated optical emission spectra around the OH line at 309.6 nm for determining the rotational temperature of (a) the cross-field jet and (c) the linear-field jet. A Boltzmann plot method was used to estimate the excitation temperature of (b) the cross-field jet and (d) the linear-field jet.

mum of 34.4 mW/cm^2 about 1.2 mm outside the quartz tube at z=6.2 mm. Beyond this point, it undergoes a gradual decay to 29.5 mW/cm^2 at z=10 mm. This is 5.9-fold of 5.0 mW/cm^2 in the cross-field case and is likely to translate into a greater application efficiency. It is worth noting that the linear-field jet in Fig. 1(b) has a more uniform visual appearance than that indicated in Fig. 1(c). This is because optical emission in Fig. 1(c) includes shorter wavelengths outside the visible range.

The monotonic decay of the cross-field jet in Fig. 1(c) is a result of a spatially confined gas ionization in the intraelectrode region. The rapid oscillation of the rf excitation voltage imparts a radially directed momentum on electrons, making it difficult for electrons to be transported axially toward the downstream region. In the linear-field jet, however, the electric field is largely in the axial direction and hence imparts an axially directed momentum to electrons. This drives an axial electron transportation to the downstream region and is critical for producing a longer and more reactive plasma plume. The decay in its optical intensity is at a rate of 3.7% per mm from 34.4 mW/cm^2 at z=6.2 mm to 29.5 mW/cm^2 at z=10 mm, and this lack of sensitive spatial dependence is desirable for achieving reproducible application efficiency particularly when precision processing is important. The appearance of the maximum intensity outside the quartz tube rather than within the electrode region is probably related to additional ionization mechanisms (e.g., photon ionization) when the plasma plume is populated with sufficiently energetic electrons.[11,12] These make the linear-field jet better suited for efficient and reliable applications in the downstream region. It is however worth noting that the cross-field jet has intense emission and so large electric field in its electrode region, making it useful for ionizing gases of large breakdown voltage, similar to a previous finding.[8]

To see reactive plasma species delivered to the application point, the optical emission spectra of both APGD jets at z=10 mm are shown in Fig. 2. They are rich in strong helium, nitrogen, oxygen, and hydroxyl lines as a result of the helium plasma jets interacting with the ambient air. The peak around 618.9 nm is due to grating orders of OH line at 309.6 nm and labeled with parentheses. It is clear that the linear-field jet has significantly stronger emission atomic O lines at 631.0, 777.4, and 844.6 nm, O_2^+ line at 533.2 nm, and OH line at 309.6 nm, which are known enablers for polymeric surface modification.[4,13,14] In particular, the intensity of the excited O atom line at 777.4 nm in the linear-field jet is 6.1-fold of that in the cross-field jet, similar to the 5.9-fold in wavelength-integrated intensity. Also notable from Fig. 2 is that the strongest emission is the N_2^* lines at 337.2 and 358.4 nm in the cross-field jet, whereas in the linear-field jet it is the excited O atom line at 777.4 nm, suggesting a difference in their electron energy distribution function (EEDF). The stronger UV emission below 300 nm in Fig. 2(b) indicates that the linear-field jet is likely to have more energetic electrons than the cross-field jet. While their EEDF may be probed further with appropriate line ratio methods,[15] it is evident that the linear-field jet offers a more active downstream plasma chemistry.

Gas temperature is an important parameter in any plasma processing application, and for atmospheric plasmas it is close to rotational temperature.[2,7–14] To determine gas temperature experienced by the material to be treated, a polyamide film was placed at z=10 mm and the measured spectrum obtained there was used to find its best-fit simulated spectrum to deduce the rotational temperature. Figures 3(a) and 3(c) show that the cross-field and linear-field APGD jets had a rotational temperature of 410 and 520 K respectively at the polyamide surface. The lower gas temperature of the cross-field jet is consistent with its weaker optical emission in the downstream region [see Figs. 1(a) and 2(a)]. For the linear-field jet, gas temperature at 520 K is markedly lower than 600 K at which polyamide remains uncompromised thermally.[16] This suggests that any potential etching effect achieved by both APGD jets is likely to be nonthermal and dependent mostly on reactive species particularly oxygen species.[4] Also shown in Fig. 3 is the excitation temperature of each jet calculated using a Boltzmann plot method applied to several excited helium emission lines.[17] Using a linear fit, the excitation temperature was found to be 0.95 and 0.99 eV, respectively, for the cross-field and the linear-field jets. As the excitation temperature may be used as a rough indication of the electron temperature,[17] these results suggest that the linear-field jet can achieve a higher mean electron energy, thus supporting the findings observed in Figs. 1 and 2.

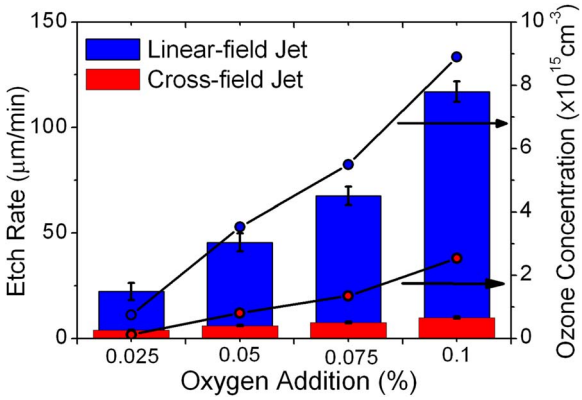

FIG. 4. (Color online) Etch rate of polyamide film measured ozone density for the cross-field jet (red) and the linear-field jet (blue) at a fixed rf input power of 15 W.

As an acid test of the findings that the linear-field jet is likely to facilitate more active plasma chemistry and larger electron mean energy, each of the two plasma jets was used to etch a 100 μm polyamide film commonly used in the semiconductor fabrication industry.[18] With a fixed input rf power at 15 W and under the same condition as those in Figs. 1–3, the etching results are shown in Fig. 4. It is clear that the linear-field APGD jet was able to achieve an etching rate of 118 μm/min or 2 μm/s at a 0.1% O_2 admixture of the carrier helium gas. This is more than 13-fold of 9 μm/min achieved with the cross-field jet at the same O_2 admixture. To compare the etching rate of the cross-field jet to that of a similar cross-field jet generated in an Ar/O_2 flow at 150 W/cm^3 and 13.56 MHz,[18] the plasma volume of the former was estimated to be approximately 0.14 cm^3 and the power density was 15/0.14=107 W/cm^3. In the Ar/O_2 case, every percentage point in the O_2 admixture resulted in an etch rate of 0.8 μm/s with a linear relationship.[18] Therefore at $O_2/Ar=0.1\%$, the etch rate would be 0.08 μm/s or 4.8 μm/min. This is at the same order of magnitude of 9 μm/min achieved with our cross-field jet, and may be regarded as indicative of the current etching capability of cross-field plasma jets. The 13-fold improvement in the etching rate achieved with the linear-field jet in Fig. 4 is therefore a generic advantage of most linear-field APGD jets because of their ability to enable more active plasma chemistry and larger electron mean energy in the downstream region. Also shown in Fig. 4 is the ozone concentration measured at $z=10$ mm using an UV absorption method at 253.7 nm. The O_3 concentration was found to be 9.0×10^{15} and 2.5×10^{15} cm^{-3} for the linear-field and cross-field jets, respectively, and the cross-field jet figure is similar to 1.0×10^{15} cm^{-3} measured in the afterglow of the Ar/O_2 jet.[18] Data of polymer etching[18] and biomolecule removal[19] have both supported the prevailing hypothesis that ground-state oxygen atoms are the main application enabler. However the difficulty of their measurement[20] has led to our use of O_3 as an alternative indicator. The etch rates of the two He/O_2 jets in Fig. 4 and the reported Ar/O_2 jet are in broad agreement with their corresponding O_3 concentrations, thus offering further support to the main conclusion of this study that the linear-field APGD jets are better suited for treatment of polymers.

In conclusion, an experimental study has been presented to demonstrate that linear-field APGD jets are capable of more active plasma chemistry and larger electron mean energy in the downstream region. This has been further supported by a 13-fold increase in the etching rate of the linear-field jet over that of its cross-field counterpart. While He/O_2 rf APGD jets were used to arrive at the conclusion, it should be generally applicable to other APGD jets employing different gas mixtures[18,20,21] or temporal excitations[1,22–24] as the interaction of the electric and flow fields appears to impose a stronger influence on downstream plasma dynamics.

[1] M. Laroussi and T. Akan, Plasma Processes Polym. **4**, 777 (2007).
[2] F. Iza, G. J. Kim, S. M. Lee, J. K. Lee, J. L. Walsh, Y. T. Zhang, and M. G. Kong, Plasma Processes Polym. **5**, 322 (2008).
[3] H. Koinuma, H. Ohkubo, T. Hashimoto, K. Inomata, T. Shiraishi, A. Miyanaga, and S. Hayashi, Appl. Phys. Lett. **60**, 816 (1992).
[4] A. Schutze, J. Y. Jeong, S. E. Babayan, J. Park, G. S. Selwyn, and R. F. Hicks, IEEE Trans. Plasma Sci. **26**, 1685 (1998).
[5] I. E. Kieft, E. P. van der Laan, and E. Stoffels, New J. Phys. **6**, 149 (2004).
[6] M. Teschke, J. Kedzierski, E. G. Finantu-Dinu, D. Korzec, and J. Engemann, IEEE Trans. Plasma Sci. **33**, 310 (2005).
[7] X. T. Deng, J. J. Shi, G. Shama, and M. G. Kong, Appl. Phys. Lett. **87**, 153901 (2005).
[8] R. Foest, E. Kindel, A. Ohl, M. Stieber, and K. D. Weltmann, Plasma Phys. Controlled Fusion **47**, 525 (2005).
[9] D. B. Kim, J. K. Rhee, B. Gweon, S. Y. Moon, and W. Choe, Appl. Phys. Lett. **91**, 151502 (2007).
[10] X. Lu, Z. Jiang, Q. Xiong, Z. Tang, and Y. Pan, Appl. Phys. Lett. **92**, 151504 (2008).
[11] X. Lu and M. Laroussi, J. Appl. Phys. **100**, 063302 (2006).
[12] J. J. Shi, F. C. Zhong, J. Zhang, and M. G. Kong, Phys. Plasmas **15**, 013504 (2008).
[13] T. Ichiki, R. Taura, and Y. Horiike, J. Appl. Phys. **95**, 35 (2004).
[14] J. L. Walsh and M. G. Kong, Appl. Phys. Lett. **91**, 251504 (2007).
[15] C. M. O. Mahony, T. Gans, W. G. Graham, P. D. Maguire, and Z. Lj. Petrović, Appl. Phys. Lett. **93**, 011501 (2008).
[16] MATWEB: Online Materials Property Database.
[17] D. Staack, B. Farouk, A. Gutsol, and A. Fridman, Plasma Sources Sci. Technol. **17**, 025013 (2008).
[18] M. Moravej, X. Yang, R. F. Hicks, J. Penelon, and S. E. Babayan, J. Appl. Phys. **99**, 093305 (2006).
[19] X. T. Deng, J. J. Shi, and M. G. Kong, IEEE Trans. Plasma Sci. **34**, 1310 (2006).
[20] K. Niemi, V. Schulz-von der Gathen, and H. F. Dobele, Plasma Sources Sci. Technol. **14**, 375 (2005).
[21] C. Cheng, Z. Liye, and R. Zhan, Surf. Coat. Technol. **200**, 6659 (2006).
[22] J. L. Walsh and M. G. Kong, Appl. Phys. Lett. **91**, 221502 (2007).
[23] J. L. Walsh, J. J. Shi, and M. G. Kong, Appl. Phys. Lett. **88**, 171501 (2006).
[24] M. Laroussi and X. Lu, Appl. Phys. Lett. **87**, 113902 (2005).